Nilsson-SU3 self-consistency in heavy $N = Z$ nuclei

A. P. Zuker,[1] A. Poves,[2,3] F. Nowacki,[1] and S. M. Lenzi[4]

[1]*Université de Strasbourg, IPHC, CNRS, UMR7178, 23 rue du Loess 67037 Strasbourg, France*
[2]*Departamento de Física Teórica e IFT-UAM/CSIC, Universidad Autónoma de Madrid, 28049 Madrid, Spain*
[3]*ISOLDE, CERN, CH-1211 Genève, Switzerland*
[4]*Dipartimento di Fisica e Astronomia dell'Università and INFN, Sezione di Padova, I-35131 Padova, Italy*

It is argued that there exist natural shell-model spaces optimally adapted to the operation of two variants of Elliott's SU3 symmetry that provide accurate predictions of quadrupole moments of deformed states. A self-consistent Nilsson-like calculation describes the competition between the realistic quadrupole force and the central field, indicating a *remarkable stability of the quadrupole moments*—which remain close to their quasi- and pseudo-SU3 values—as the single-particle splittings increase. A detailed study of the $N = Z$ even nuclei from ^{56}Ni to ^{96}Cd reveals that the region of prolate deformation is bounded by a pair of transitional nuclei ^{72}Kr and ^{84}Mo in which prolate ground-state bands are predicted to dominate, though coexisting with oblate ones.

I. INTRODUCTION

Large-scale shell model (LSSM) calculations, when numerically feasible, are the spectroscopic tool of choice in theoretical nuclear structure. When they are not doable it is often advised to switch to other—basically mean-field—methods. A common feature of these approaches is the reliance on quadrupole degrees of freedom as the backbone of nuclear structure, which in shell-model language translates as dominance of the quadrupole force, which is indeed (or should be) a classic view. Our task is to find ways to put to good use this dominance. It starts by discovering which are the model spaces in which to operate. The choice turns out to be quite unique (the extended extruder-intruder spaces to be defined soon). Though most often it leads to intractably large diagonalizations, it also happens to be tailored to take full advantage of two variants—pseudo- and quasi-SU3—of Elliott's SU3 symmetry [1]. After explaining in detail how these symmetries operate, we turn to quantitative estimates of their reliability by defining and implementing a self-consistent Nilsson [2] approach in which the interplay of a realistic quadrupole interaction with the spherical central field establishes the resilience of the predicted quadrupole moments. The controlling parameters are the quadrupole moments themselves, which, in the absence of a central field, reduce to one of their SU3-like guises.

These ideas are applied to the heavy even $N = Z$ nuclei shedding light on the hitherto poorly understood competition between prolate and oblate quadrupole coherence. In this region the full interplay of quasi- and pseudo-SU3 schemes operates, illustrating what will become the rule for well-deformed nuclei, so far only schematically explored at the onset of rotational motion at $N = 90$ [3].

II. THE NATURAL ZBM (OR EEI) MODEL SPACES

The usual lore about shell-model spaces is that for light and medium nuclei they involve one major oscillator (HO) shell bounded by magic numbers at $N, Z = 4, 8, 20$, and 40, while for heavier systems the spin-orbit (SO) force takes over and the magic boundaries move to $N, Z = 28, 50, 82$, and 126. This

view has some merit but misses two crucial points: (a) The observed shell evolution is not driven by the SO terms present in the NN interactions, but by three-body forces (a word on this later); (b) the correct model spaces are larger than those defined by the SO boundaries. Let us examine the possible examples.

In the p shell starting at ^{4}He, as particles are added the largest orbit $p_{3/2}$ is "extruded" (or ejected or expelled) from the space by becoming a "closed shell" when filled, while the largest orbit in the next shell "intrudes" so as to define the first of the "EI" spaces $p_{1/2}d_{5/2} \equiv r_1 d$ (closing at ^{28}Si). The notation r_p stands for "rest of the major shell of principal quantum number p," i.e., all the orbits except the largest one. What we miss here is that the $d_{5/2}$ intruder does not come alone but with an $s_{1/2}$ partner, as made evident by the spectrum of ^{13}C [4]. Therefore, the correct space is the first of the extended EI spaces: $r_1 ds$ (EEI1 or ZBM [5]), with $ds = d_{5/2}s_{1/2}$, which is the first instance of a "$\Delta j = 2$" sequence.

Notation. The full harmonic oscillator shells are called $sd, pf, sdg, \ldots$, while the reverse order $ds, fp, gds, \ldots$ is used for the $\Delta j = 2$ sequences.

The next candidate comes from the sd shell starting at ^{16}O, where, as it fills, $d_{5/2}$ is separated from its partners while drawing down the largest orbit in the next shell so as to define the EI2 space: $s_{1/2}d_{3/2}f_{7/2} \equiv r_2 f$ (starting at ^{28}Si and closing at ^{56}Ni). However, we miss again that the intruder comes with its $\Delta j = 2$ partner (as seen in ^{29}Si [4]), so $r_2 f$ becomes $r_2 fp$ (EEI2 or ZBM2), with $fp = f_{7/2}p_{3/2}$. Then we find the space, relevant for this study, $p_{1/2}p_{3/2}f_{5/2}g_{9/2} \equiv r_3 g$ (EI3 closing at ^{100}Sn), which is expected to become $r_3 gds$ (EEI3 or ZBM3), with $gds = g_{9/2}d_{5/2}s_{1/2}$. Direct experimental evidence of the presence of the $\Delta j = 2$ partners is hard to obtain in this region, but abundant indirect evidence is presented in this paper.

One objection to the description above is that ^{12}C and ^{28}Si are not closed shells (though ^{56}Ni is to a good approximation). However, EI numbers at $N, Z = 6, 14, 28, 50, 82$, and 126 provide good boundaries and many convincing candidates to magicity in the light nuclei (such as ^{14}C, ^{22}O, and ^{34}Si) and the *only* systematic magic numbers beyond. The transition from HO to EI major closures demands three-body mechanisms
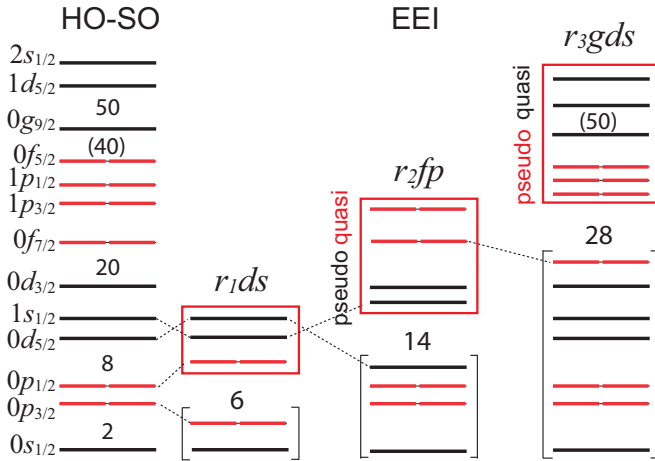
FIG. 1. (Color online) Evolution of model spaces from spin-orbit (SO) (around HO closures) to extended extruder-intruder (EEI) made of pseudo-SU3 and quasi-SU3 subspaces (explained in Sec. III).

FIG. 2. (Color online) Eigenstates of $-2q_{20}$. SU3 intrinsic states of minimum energy are obtained by orderly filling. Note that $-Q_0$ is plotted on the vertical axis.

whose irrefutable need is now established on theoretic [6] and empiric [7,8] grounds. Explicit introduction of three-body forces (Fig. 3(b) vs Figs. 3(c) and 3(d) in Ref. [9]) helps but does not explain the strong magicity of ^{22}O, as seen by comparing the quoted figures. The notation EI instead of the usual SO is meant to stress that the SO force—in the classic $l \cdot s$ sense—is perfectly given by existing NN interactions above HO closures, where it is responsible for the largest orbit coming lowest [10]. However, it is definitely not responsible for the EI closures which demand splittings much larger that the $l \cdot s$ one provided by the NN interactions. To fix ideas, in ^{48}Ca they would produce a $f_{7/2}$-$p_{3/2}$ single-particle gap equal to that in ^{41}Ca, i.e., 2.5 MeV smaller than the observed one, a discrepancy that increases to some 4.5 MeV in ^{56}Ni. The evolution of subshell SO ordering on top of HO closures to the EEI patterns is illustrated in Fig. 1 for different model spaces.

Both r_1ds (ZBM) and r_2fp (ZBM2 or SDFP) models lead to feasible and successful diagonalizations in the neighborhood of ^{16}O and ^{40}Ca [5,11]. The r_3gds space is expected to work equally well around ^{80}Zr—formally the magic upper boundary of the pf shell—which turns out to be a splendid rotor [12]. A pure pf description starts failing around $N,Z \approx$ 34, and it could be hoped that r_3g would cope beyond, but the calculations (always feasible though sometimes hard) fail to produce strongly deformed prolate bands demanded by the data. These are naturally explained in the r_3gds space, as we shall demonstrate notwithstanding the near impossibility of exact diagonalizations: first through heuristic arguments based on the approximate SU3 symmetries and then by very simple self-consistent calculations that account semiquantitatively for the interplay between the realistic quadrupole interaction and the monopole central field.

III. QUADRUPOLE COHERENCE: SU3, PSEUDO-SU3, AND QUASI-SU3

Nuclear rotational motion was predicted by Bohr and Mottelson in 1953 [13]. The idea was that nuclei could acquire a permanent quadrupole deformation in their intrinsic
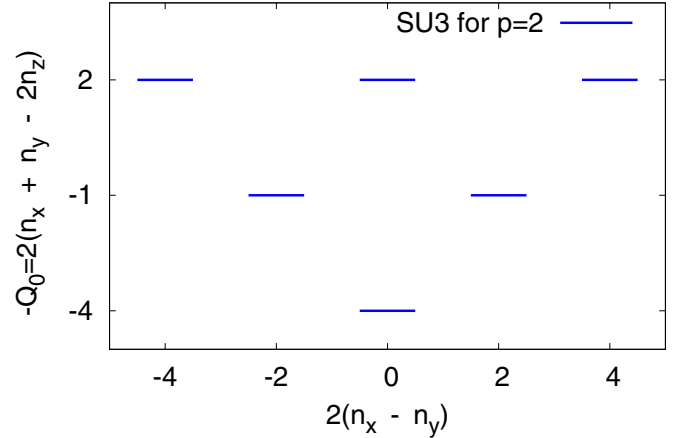
frame, which would translate into a $J(J + 1)$ spectrum in the laboratory frame. Historically, this first example of spontaneously broken symmetry was confronted with the need to explain how a deformed intrinsic state—which has no definite angular momentum J—could be an eigenstate of a system that must necessarily conserve J. The elegant way out was found by Elliott, whose SU3 model [1] provides a rigorous example of intrinsic states that are not eigenstates of a Hamiltonian H but of $H - \lambda J(J + 1)$.

More precisely, H is taken to be the quadrupole force $-2q \cdot 2q$, with $q \equiv q^{2m} = r^2 C^{2m} = r^2 \sqrt{4\pi/5}\, Y^{2m}$ acting in a full major HO shell. Then the eigenstates have the form $E(L,i) = E(i) + 3L(L + 1)$, where L is the orbital angular momentum and $E(i)$ the energy of one of the possible intrinsic states. We are interested only in those that maximize the intrinsic quadrupole moment, which we write in terms of oscillator quanta $Q_0 = 2q^{20} = (2n_z - n_x - n_y)$. Taking, for example, $p = n_x + n_y + n_z = 2$, the six possible single-particle states $[n_z n_x n_y] = [200],[110],[101],[020],[011],[002]$ can be disposed as in Fig. 2. The intrinsic states are the determinants obtained by filling the fourfold degenerate orbits (two neutrons and two protons of spins up and down) from below (prolate states with $Q_0 > 0$) or from above (oblate states with $Q_0 < 0$). Prolate filling is favored as it leads to larger $|Q_0|$.

Originally, SU3 was expected to apply to the sd shell. Indeed, the four particles in ^{20}Ne ($Q_0 = 16$) produce a good rotor and eight particles in ^{24}Mg—because of the degeneracy of the $Q_0 = 1$ levels in Fig. 2—lead to triaxiality, associated with the mixing of $K = 0$ and $K = 2$ prolate bands. For 12 particles in ^{28}Si, both shapes are expected to be degenerate ($|Q_0| = 24$). Observation does not quite square with predictions: The $K = 2$ band in ^{24}Mg is higher than expected, and the "nearly degenerate" oblate and prolate states in ^{28}Si are separated by some 6 MeV with a third candidate coming in (the $d_{5/2}^{12}$ $N = Z = 14$ closure in Fig. 1). Still, the departure from strict SU3 validity should not hide the fact that ^{24}Mg has a $K = 2$ (γ) band, and that three of the six lowest states in ^{28}Si have $J = 0^+$, a forerunner of other spectacular coexistence situations.

Though Elliott's conceptual breakthrough was obscured by the limited applicability of the exact SU3 symmetry, its indicative value remains high, as illustrated by examining the possible forms of the q^{20} operator in LS and jj formalisms in Eqs. (1)–(5): They will be seen to suggest naturally the pseudo- and quasi-SU3 variants that are the backbone of a full shell-model description of rotational motion:

$$\langle pl|r^2|pl\rangle = p + 3/2, \tag{1}$$

$$\langle pl|r^2|pl + 2\rangle = -[(p - l)(p + l + 3)]^{1/2}, \tag{2}$$

$$\langle lm|C_2|lm\rangle = \frac{l(l+1) - 3m^2}{(2l+3)(2l-1)}, \quad \langle lm|C_2|l+2m\rangle$$
$$= \frac{3}{2}\left\{\frac{[(l+2)^2 - m^2][(l+1)^2 - m^2]}{(2l+5)(2l+3)^2(2l+1)}\right\}^{1/2}, \tag{3}$$

$$\langle jm|C_2|jm\rangle = \frac{j(j+1) - 3m^2}{2j(2j+2)}, \quad \langle jm|C_2|j+2m\rangle$$
$$= \frac{3}{2}\left\{\frac{[(j+2)^2 - m^2][(j+1)^2 - m^2]}{(2j+2)^2(2j+4)^2}\right\}^{1/2}, \tag{4}$$

$$\langle jm|C_2|j+1m\rangle = -\frac{3m[(j+1)^2 - m^2]^{1/2}}{j(2j+4)(2j+2)}. \tag{5}$$

Intrinsic states can be constructed by diagonalizing q^{20}, which can be done in three possible ways, described next, after noting that, so far, we have assumed dimensionless oscillator coordinates and made no difference between $\langle 2q^{20}\rangle$ and Q_0. Dealing with electromagnetic properties demands to recover dimensions so $r^2 \to r^2 b^2$, where b^2 is the oscillator parameter. Then $Q_0 \to Q_0 b^2$. However, $\langle 2q^{20}\rangle$ is best kept adimensional when working with the quadrupole interaction. So now $Q_0/b^2 = \langle 2q^{20}\rangle$, and the choice of notation will depend on context.

A. Strict SU3

Use Eqs. (1)–(3) in LS form to obtain exactly Fig. 2. Alternatively, use Eqs. (1), (2), (4), and (5) in jj form to incorporate spin, leading to the bottom panel of Fig. 3. Only positive values of $K \equiv |m|$ are shown. Each orbit may contain two neutrons and two protons. Note that if in Fig. 2 spin is allowed each orbit splits into $2(n_x - n_y) \equiv 2m \to 2(m \pm 1/2)$ and the one-to-one correspondence with the bottom panel of Fig. 3 becomes evident.

The importance of SU3 goes well beyond its mathematical elegance: It rests on the introduction of the $q \cdot q$ interaction restricted to a single major HO shell, which, as demonstrated in Ref. [14], is the major collective ingredient of realistic Hamiltonians (i.e., consistent with two nucleon data).

B. Pseudo-SU3

Pseudo-SU3 [15] is adapted to r_p spaces whose orbits have the same angular momentum j sequences as those of full HO major shell with total quantum number $p - 1$ and proceeds as if $r_p \equiv HO(p - 1)$, in our case $r_3 \equiv sd$. For the angular
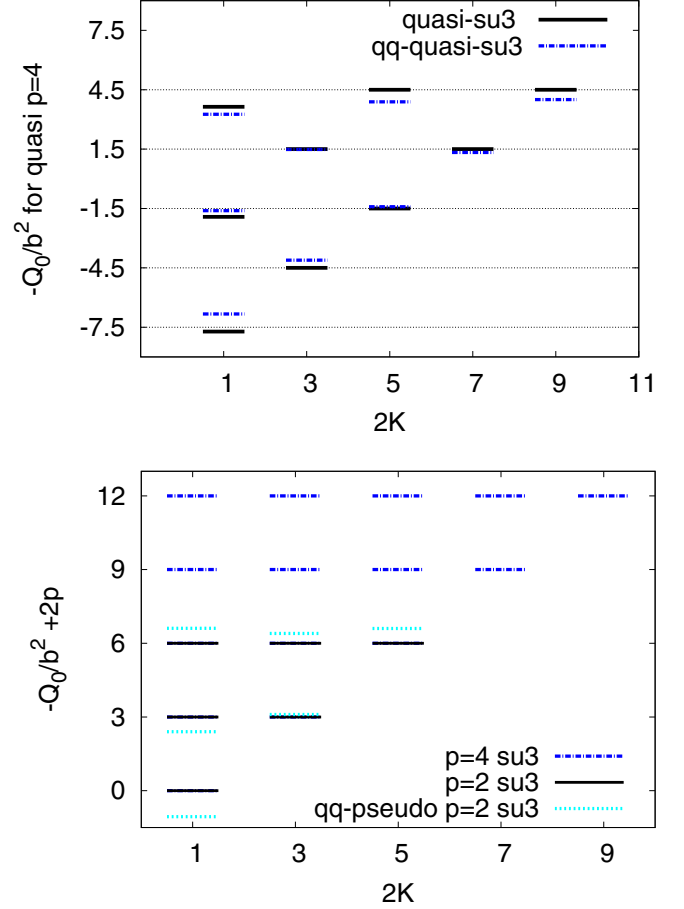

FIG. 3. (Color online) The Zuker-Retamosa-Poves (ZRP) diagrams. (Top) Intrinsic states in the $p = 4$ gds space for the quasi-SU3 model and for the exact $q \cdot q$ calculation. See text for explanation of thin lines. (Bottom) Intrinsic states of SU3 or pseudo-SU3 for $p = 2$ and 4. For the former, exact $q \cdot q$ values ("qq-pseudo") are also shown. Each orbit may contain two neutrons and two protons. The lowest six orbits are common to $p = 2$ and 4.

Eqs. (4) and (5) the identity is perfect but the radial Eqs. (1) and (2) raise a problem: r_3 has $p = 3$ and sd has $p = 2$. The bottom panel of Fig. 3 exhibits both of the strict SU3 (or pseudo-SU3) values for $p = 2$ and 4, as well as the exact result of diagonalizing $2q^{20}$ in the r_3 space, collected under p-d in Table I. It is seen that the differences are substantial, but they do not invalidate the existence of an underlying SU3 symmetry: The $q \cdot q$ interactions in the sd and r_3 spaces are very different, but their behavior is qualitatively similar. In what follows we always use the exact r_3 variant of $q \cdot q$.

C. Quasi-SU3

Quasi-SU3 [3,16] is adapted to $\Delta j = 2$ spaces. Then $\langle jm|C_2|j+1m\rangle$ in Eq. (5) plays no role. Now identify the $\Delta j = 2$ sequence to a $\Delta l = 2$ one. In our case it is $J = 9/2, 5/2, 1/2$ to $l = 4, 2, 0$. Then replace Eqs. (1), (2), and (4) with Eqs. (1), (2), and (3), through $l \to j$, $p \to p + 1/2$, $m \to m + 1/2$, and $-m \to -m - 1/2$: ($m > 0$). This defines a quasi-q_{20} operator whose spectrum is shown (under "quasi-

TABLE I. Eigenvalues of $-2q^{20}$ for the ith quasi-gds (denoted q) and pseudo-r_3 (denoted p) orbits; q-s, p-s are the results using the schematic quasi- and pseudoquadrupole forces, respectively, in Fig. 3. q-d and p-d are the results of diagonalizing the exact quadrupole interaction; c-q and c-p are the corresponding cumulated absolute values for n particles in units of b^2.

i	1	2	3	4	5	6	7	8	9
q-s	-7.71	-4.50	-1.92	-1.50	1.50	1.50	3.64	4.50	4.50
q-d	-6.83	-4.11	-1.61	-1.42	1.33	1.48	3.26	3.90	4.00
p-s	-4.00	-1.00	-1.00	2.00	2.00	2.00			
p-d	-5.06	-1.41	-1.08	2.37	2.57	2.61			
			Q_0 values for n particles (c-q for gds and c-p for r_3)						
n	4	8	12	16	20	24	28	32	36
c-q	27.32	43.76	50.20	55.88	50.56	44.64	31.60	16.00	0.00
c-p	20.24	25.88	30.20	20.72	10.44	0.00			

su3") in the top panel of Fig. 3, where thin lines indicate a one-to-one correspondence with Fig. 2, with bandheads at $2p - 1/2$, except for $K = 1/2$ for even p. For odd p the correspondence is perfect throughout. The spectrum for the genuine q^{20} operator ("qq-quasi-su3" in the figure) is seen to be quite close to the schematic one (numerical values are collected under q-d in Table I).

Table I compares the schematic orbits of Fig. 3 with the ones obtained by diagonalizing $2q^{20}$ associated with "true" $2q \cdot 2q$ and not one of its variants. The two bottom lines give the cumulated values after filling up to ith orbit with two neutrons and two protons. Thus, for 12 particles in r_3 and 4 in gds we find $\langle 2q^{20} \rangle = 30.20 + 27.32 = 50.52$. This table is the relevant one for prolate states.

Quasi-SU3 strongly prefers prolate solutions, as Fig. 3 makes clear: It is more advantageous to fill orbits from below than from above.

D. Single-orbit quadrupole

When the g orbit becomes sufficiently depressed with respect to its ds partners their influence can be neglected and we move to the single j orbit regime with quadrupole moments given by

$$Q_0 = 2\langle r^2 C_2 \rangle = \sum_m (p + 3/2) \frac{j(j+1) - 3m^2}{2j(j+1)}, \quad (6)$$

which shows that, before midshell, filling large m values (negative Q_0) is favored. The situation is reversed after midshell. Though the notion of shape is questionable in this case, states with positive and negative Q_0 are referred to as prolate and oblate, respectively.

Table II collects the possible values of $\langle 2q^{20} \rangle$ for the $g_{9/2}$ orbit and the r_3 space, where one may wish to speak in terms of holes rather than particles, and the table allows for all possibilities. For example, under $\mu = 8$ we find that $\langle 2q^{20} \rangle = 25.88$ for prolate particles, 20.72 for prolate holes, -25.88 for oblate holes, and -20.72 for oblate particles.

To guarantee a *bona fide* intrinsic state, Q_0 must coincide with the values extracted either from the spectroscopic quadrupole moment (Q_{0s}),

$$Q_{\text{spec}}(J) = \langle JJ|3z^2 - r^2|JJ \rangle,$$

$$Q_{0s} = \frac{(J+1)(2J+3)}{3K^2 - J(J+1)} Q_{\text{spec}}(J), \quad K \neq 1, \quad (7)$$

for Bohr Mottelson rotors or the corresponding $B(E2)$ transitions (Q_{0t}),

$$B(E2, J \rightarrow J - 2) = \frac{5}{16\pi} e^2 |\langle JK20|J-2, K \rangle|^2 Q_{0t}^2,$$

$$K \neq 1/2, 1. \quad (8)$$

The condition $Q_0 \approx Q_{0s} \approx Q_{0t}$ is well fulfilled by SU3 states and its variants. (Q_{0s} may be tricky, though, as it is more sensitive to details than Q_{0t}. For an example, refer to Sec. VA2.)

IV. COMPUTATIONAL STRATEGY: SU3-NILSSON SELF-CONSISTENCY

The guiding idea is that once quadrupole dominance sets in, the wave functions are basically given by the quadrupole force, which is quite immune to single-particle details. In other

TABLE II. (Top) Intrinsic prolate and oblate quadrupole moments $\langle 2q^{20} \rangle$ for ν particles in the $0g_{9/2}$ orbit ($N = Z$). (Bottom) Pseudo-SU3 $\langle 2q^{20} \rangle$ for μ prolate particles (p-p) or μ prolate holes (p-h), $-\langle 2q^{20} \rangle$ for μ oblate particles [-(o-p)] or μ oblate holes [-(o-h)].

ν	2	4	6	8	10	12	14	16
prol	5.33	10.66	14.66	18.66	20	21.33	18.66	16
$-$obl	8	16	18.66	21.33	20	18.66	14.66	10.66
μ	2	4	6	8	10	12	14	16
p-p; -(o-h)	10.12	20.24	23.04	25.88	28.05	30.20	25.46	20.72
p-h; -(o-p)	5.22	10.44	15.66	20.72	25.46	30.20	28.04	25.88

words, $\langle 2q^{20} \rangle$ varies little. Our aim is to estimate $\langle 2q^{20} \rangle$ and understand the reason for its stability.

We are interested in even $N = Z = 28$ to 48 nuclei. Full pf diagonalizations are possible, but their interest is restricted to the lightest species. For $r_3 g$ exact calculations are also possible that account for oblate states. The JUN45 interaction [17] is used throughout the region. Though the $r_3 g$ space is of limited relevance, the exact calculations serve as a test of our simple models. For the more collective prolate states the full $r_3 g d s$ space is necessary and exact calculations are not presently feasible, so we introduce a self-consistent version of Nilsson's model that reduces to quasi- and pseudo-SU3 in the absence of a central field [18].

A. Example of naive $BE2$ estimate

For SU3 the correct value of Q_0 to be used in Eqs. (7) and (8) is $Q_0 = (\langle 2q^{20} \rangle + 3) b^2$ [1,19] with $\langle 2q^{20} \rangle$ given in Table I or II. In what follows we adopt this form in all cases.

The procedure is simple: Use the tables to match oblate pseudo-SU3 states in r_3 to oblate states in g and prolate pseudo-SU3 states in r_3 to prolate quasi-SU3 states in gds. For instance, choose 16 particles and decide that we are interested in ^{72}Kr configurations with 12 particles in r_3 and 4 above. From the tables we have for $\langle 2q^{20} \rangle$ the following possibilities:

. Oblate
   $\langle 2q^{20} \rangle = -30.2$ for $m = 12$ in pseudo,
   $\langle 2q^{20} \rangle = -16$ for $n = 4$ in g,
   Total $Q_0 / b^2 = -(30.2 + 3 + 16) = -49.2$;
   Prolate
   $\langle 2q^{20} \rangle = 30.2$ for $m = 12$ in pseudo,
   $\langle 2q^{20} \rangle = 27.32$ for $n = 4$ in quasi,
   Total $Q_0 / b^2 = 30.2 + 3 + 27.32 = 60.52$;
   Recover dimensions through $b^2 \approx 41.4 / \hbar\omega$ fm^2, $\hbar\omega = 45 A^{-1/3} - 25 A^{-2/3}$.

Now assume a conventional $2\hbar\omega$ scalar effective charge, $e_0 = e_\nu + e_\pi = 2$ *chosen throughout in what follows*. Then, for $A = 72$, $b^2 = 4.42$ e fm^2, we have $Q_0 \approx -217$ e fm^2 (oblate) and 267 e fm^2 (prolate).

The $2\hbar\omega$ effective charge is caused by coupling states in a major HO shell to the giant quadrupole resonance. A rigorous derivation leads $e_0 = 1.77$ [14], a number to be preferred [20], and shown in parentheses below. Using $B(E2 : 2^+ \to 0^+) = [Q_0]^2 / 50.3$ from Eq. (8) leads to
$B(E2 : 2^+ \to 0^+) \approx 936(725)$ e^2 fm^4 for oblate;
$B(E2 : 2^+ \to 0^+) \approx 1422(1101)$ e^2 fm^4 for prolate.

When working in EI or EEI spaces it becomes necessary to account for $0\hbar\omega$ polarization effects, in our case owing to coupling to the lowest $J = 2^+$ state in ^{56}Ni. The effect is estimated later, leading to $e_0 \gtrsim 2$.

B. Nilsson revisited: The MZ equations

The estimates above neglect single-particle effects. To account for them demands solving the Schrödinger equation for the quadrupole force in the presence of a central field, a task

as hard as the general problem. In Ref. [16] Martínez-Pinedo and Zuker (MZ) proposed to reduce it, by linearization, to a Nilsson-type Hamiltonian. That this should be possible seems obvious, but the implementation is not trivial. Because of a subtlety that was missed at the time, the project was left unfinished. We retake it.

We would like to solve

$$H_{mq} = \sum \epsilon_i n_i - \hbar\omega\kappa \left(\frac{2q_p}{\mathcal{N}_{2q,p}} + \frac{2q_{p+1}}{\mathcal{N}_{2q,p+1}} \right)^2, \quad (9)$$

$$\mathcal{N}_{2q,p}^2 = \sum (2q_{rs})^2 = \frac{5}{2} \sum_{k=0}^{p} (k+1)(2p - 3k)^2, \quad (10)$$

where we have borrowed from Ref. [14] the normalized form of the quadrupole force that emerges naturally when it is extracted from a realistic interaction (q_p is the quadrupole operator in major shell p; the square stands for scalar product). This form ensures that $\kappa \approx 0.22$–0.25 is a universal constant that demands a 30% renormalization owing to coupling to the $2\hbar\omega$ quadrupole degrees of freedom [14]. It also ensures that nuclei do not become needles, thus solving the crippling problem of the naive quadrupole force [21]. In all that follows we have fixed $\kappa = 0.3$.

To prepare for linearization replace q with q_{20} operators (notice that we use sometimes q_{20} instead of q^{20} for typographical reasons),

$$H_{mq0} = \sum \varepsilon_i n_i - \hbar\omega\kappa \left(\frac{2q_{20,p}}{\mathcal{N}_{2q_{20,p}}} + \frac{2q_{20,p+1}}{\mathcal{N}_{2q_{20,p+1}}} \right)^2, \quad (11)$$

$$\mathcal{N}_{2q_{20,p}}^2 = \sum (2q_{20,rs})^2 = \sum_{k=0}^{p} (k+1)(2p - 3k)^2. \quad (12)$$

Note that Eq. (12) is obtained by summing the squares of the levels in Fig. 2.

Now concentrate on a single space. The operation amounts to replacing $2q \cdot 2q$ with $2q_{20} 2q_{20}$ and demands some care because q_{20} is a sum of neutron and proton contributions $q_{20} = q_{20}^\nu + q_{20}^\pi$. As calculations are done for each fluid separately, the correct linearization for the neutron operators, say, is

$$q_{20} q_{20} \to q_{20}^\nu \langle q_{20}^\nu + 2q_{20}^\pi \rangle \approx 3q_{20}^\nu \langle q_{20}^\nu \rangle \text{ if } \langle q_{20}^\nu \rangle \approx \langle q_{20}^\pi \rangle,$$

leading to the MZ equation

$$H_{mq0} = \sum \varepsilon_i n_i - \frac{3\hbar\omega\kappa}{\mathcal{N}_{2q_{20},p}^2} \langle 2q_{20}^\nu \rangle 2q_{20}^\nu. \quad (13)$$

The subtlety missed in Ref. [16] was the need to change $\mathcal{N}_{2q,p}$ into $\mathcal{N}_{2q_{20},p}$ in going from Eqs. (9) to (11), thus making it impossible to discover the proper way to proceed, which now can be implemented [18].

To find the proper generalization of Eq. (13), note that in the full space q becomes a sum of four contributions $q_{20} = q_{20}^{\nu u} + q_{20}^{\pi u} + q_{20}^{\nu d} + q_{20}^{\pi d}$ ($u = gds$, $d = r_3$). Repeating the arguments leading to Eq. (13) and setting $\mathcal{N}_i = \mathcal{N}_{2q_{20},i}$ leads to the general
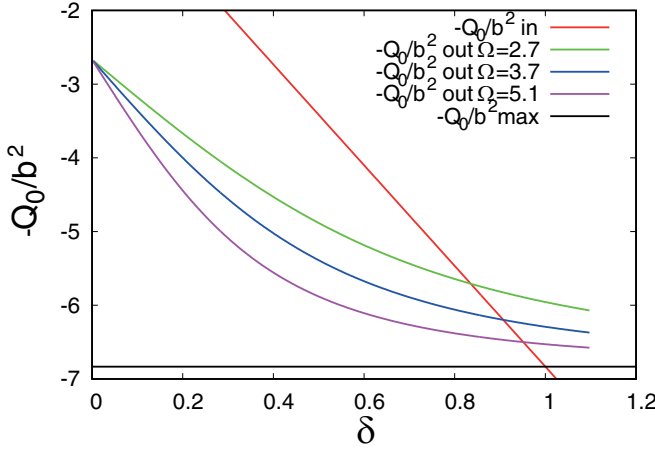
FIG. 4. (Color online) Calculation of $\langle 2q_{20} \rangle$ in $(gds)^4$. Input values are in red. Output values were obtained solving Eq. (13) for $\varepsilon_i = 0, 1, 2$ MeV for $i = g, d, s$, respectively. When input and output values coincide, self-consistency is achieved, i.e., when lines cross, which happens at abscissae 0.83, 0.91, 0.95 for $\Omega = \hbar\omega\kappa = 2.7, 3.7, 5.1$, respectively. $\delta = 0 \langle 2q^{20} \rangle = 2.666$ corresponds to one prolate g orbit (from Table II).

MZ equation

$$
\begin{aligned}
H_{\text{sp}} &- 4\hbar\omega\kappa \frac{q_4^\nu}{\mathcal{N}_4^2} \left(\langle q_4^\nu \rangle + \langle 2q_4^\pi \rangle + \langle 2q_3^\nu \rangle \frac{\mathcal{N}_4}{\mathcal{N}_3} + \langle 2q_3^\pi \rangle \frac{\mathcal{N}_4}{\mathcal{N}_3} \right) \\
&\approx H_{\text{sp}} - 4\hbar\omega\kappa \frac{q_4^\nu}{\mathcal{N}_4^2} (3\langle q_4^\nu \rangle + 6\langle q_3^\nu \rangle) \\
&= H_{\text{sp}} - \beta\hbar\omega\kappa \frac{\langle 2q_4^\nu \rangle}{\mathcal{N}_4^2} 2q_4^\nu,
\end{aligned}
\tag{14}
$$

where we have introduced a boost factor β, set $q_i^\nu = q_i^\pi$, and used the correct numbers from Eq. (12), $\mathcal{N}_{2q,3} = \sqrt{90 \times 2.5} \approx 15$, $\mathcal{N}_{2q,4} = \sqrt{210 \times 2.5} \approx 23$, to approximate $\mathcal{N}_4/\mathcal{N}_3 = 22.91/15 \approx 1.5$.

As the $\langle 2q^{20} \rangle$ ranges will be $\langle 2q_3 \rangle \approx 30$ and $\langle 2q_4 \rangle = 27$–$55$, the modest value of $\beta = 3$ in Eq. (13) will increase to about $\beta = 9$–12, but the work involved in solving Eqs. (13) and (14) is identical.

Let us examine the steps involved.

(a) Equation (13) is solved setting as inputs $\langle 2q_{20\text{in}} \rangle = \delta \langle 2q_{20\text{max}} \rangle$, which for $\delta = 1$ yields the maximum value of $\langle 2q_{20} \rangle$ (the one obtained at $\varepsilon_i = 0$). The resulting eigenvalue can be written as

$$
E(\delta) = \langle H_{\text{sp}} \rangle - \frac{3\hbar\omega\kappa}{\mathcal{N}_{2q_{20}}^2} \delta \langle 2q_{20\text{max}} \rangle \langle 2q_{20\text{out}} \rangle . x
\tag{15}
$$

(b) Extract $\langle 2q_{20\text{out}} \rangle$, use it as the next input, and iterate until $\langle 2q_{20\text{in}} \rangle = \langle 2q_{20\text{out}} \rangle$. Figure 4 sums up the procedure.

(c) Guess the energies. The comparison of the resulting $\langle 2q_{20\text{out}} \rangle = Q_0/b^2$ with exact results turns out to be systematically satisfactory. Some examples are given in Sec. IV C. As a reasonable estimate of Q_0/b^2 amounts to a good guess of intrinsic state from which the energy could be extracted by taking the expectation value of H_{mq} in Eq. (9), but it is more instructive and simpler to stand by our basic assumption that

$2q_{20}$ is an acceptable quantum number and rely on the exact SU3 result as a guide,

$$
E = -\frac{\hbar\omega\kappa}{\mathcal{N}_{2q}^2} [2\lambda(2\lambda + 6) + 2\mu(2\mu + 6) + 4\lambda\mu - 3L(L + 1)],
$$

where λ and μ are the difference in quanta in the z and x and the x and y directions, respectively. This result is valid for the $q \cdot q$ force that contains one- and two-body parts. Because we are not interested in the former, we expect modifications if they are neglected. Moreover, we restrict the energy estimates to $(\lambda 0)$ representations because the only obviously correct identification in the absence of external monopole fields is $2\lambda = \langle 2q^{20} \rangle$. The idea is to assume that the quadrupole contribution to the energy keeps this form using the calculated $\langle 2q^{20} \rangle$ value.

The proposed estimates are as follows:

$$
BE2 = B(E2 : 2^+ \rightarrow 0^+) = [(\langle 2q_{20} \rangle + 3)b^2]^2 / 50.3,
$$

$$
Q_s = Q_{(J=2)s} = (\langle 2q_{20} \rangle + 3)b^2 / 3.5,
$$

$$
E = \langle H_{\text{sp}} \rangle - \frac{\hbar\omega\kappa}{\mathcal{N}_{2q}^2} \langle 2q_{20} \rangle (\langle 2q_{20} \rangle + \zeta).
\tag{16}
$$

For Q_s and $B(E2 : 2^+ \rightarrow 0^+)$, we use Eqs. (7) and (8). The norms are those of the full quadrupole interaction; i.e., $\mathcal{N}_{2q} = \sqrt{2.5} \mathcal{N}_{2q20}$. The parameter ζ in the form of E should be 6 if the SU3 analogy held perfectly. However, as hinted above and made evident in Sec. IV C, this is not possible and ζ must be viewed as an artifact to estimate uncertainties in the guessed energies.

Finally, let us propose a generalization of Eq. (16) for the the energy of a $r_3^k (gds)^l$ configuration and write explicitly Q_s and $B(E2 : 2^+ \rightarrow 0^+)$. Calling $\langle 2q_{20(i)} \rangle = Q_i$, we have

$$
BE2 = B(E2 : 2^+ \rightarrow 0^+) = [(Q_3 + Q_4 + 3)b^2]^2 / 50.3,
$$

$$
Q_s = Q_{(J=2)s} = (Q_3 + Q_4 + 3)b^2 / 3.5,
$$

$$
E = H_m - \hbar\omega\kappa \left(\frac{Q_3}{15} + \frac{Q_4}{23} \right) \left(\frac{Q_3 + \zeta}{15} + \frac{Q_4 + \zeta}{23} \right),
\tag{17}
$$

where the monopole term H_m subsumes the evolving behavior of the single-particle fields discussed in Sec. V B.

C. Pseudo- and quasi-SU3 as exact symmetries

According to SU3, ^{28}Si has a prolate-oblate degenerate ground state corresponding to the $(\lambda, \mu) = (12, 0)$ and $(0, 12)$ representations. This holds for the full $q \cdot q$, i.e., including both its one- and two-body terms. If the former are ignored we obtain the results in the top right part of Table III, which show no signs of an exact degeneracy. The estimated energy using $\zeta = 0$ in Eq. (16) is about 5% larger than the exact one. Nearly perfect degeneracy is achieved with the monopole-free $q \cdot q$—i.e., with all centroid averages set to 0—in the top left part and the estimated energy with $\zeta = 3$ is now some 5% too small.

The story repeats itself in the bottom parts for ^{68}Se: a remarkable result establishing that pseudo-SU3 behaves as an exact symmetry in this case. This is a puzzling result because

TABLE III. $q \cdot q$ calculations in ^{28}Si $[(sd)^{12}]$ (top parts) and ^{68}Se $[r_3^{12}]$ (bottom parts). To the left, $q \cdot q$ is made monopole free. "Int" stands for intrinsic values defined in Eq. (16), with $\zeta = 3$ in the left part and 0 in the right one. Absolute energies given for the ground state; excitation energies given for the other states (MeV).

J	E	Q_s	$BE2$	J	E	Q_s	$BE2$
0	−27.263 29			0	−22.044		
0	0.001 92			2	0.958	−26.330	166.979
2	0.917 14	−0.7785	167.299	0	1.646		
2	0.917 30	0.7785	167.301	2	2.494	26.323	166.903
Int	−26.20	−26.40	169.74	Int	−23.23	−26.40	169.74
0	−14.978 22			0	−12.176		
0	0.000 42			2	0.533	−42.087	426.802
2	0.506 77	−2.8707	427.591	0	0.996		
2	0.506 83	2.8708	427.590	2	1.467	42.117	426.915
Int	−13.99	41.21	413.64	Int	−12.73	41.21	413.64

we are using the true $q \cdot q$ potential whose matrix elements coincide in magnitude with their pseudo counterparts but have different sign structure, so much so that their overlaps [in the sense of Ref. [11], Eq. (44)] nearly vanish.

Let us draw some conclusions.

(i) Energies are very sensitive to monopole behavior, but $B(E2 : 2^+ \rightarrow 0^+)$ rates are not.

(ii) When bands—with equal $B(E2 : 2^+ \rightarrow 0^+)$ and opposite Q_s—cross, they mix, leading to unchanged $B(E2 : 2^+ \rightarrow 0^+)$ and cancellation of Q_s. Note that this could happen through small "impurities" in the Hamiltonian. If the symmetry were exact, the Lanczos algorithm used in the diagonalizations could not break the degeneracy.

(iii) Pseudo-SU3 appears to be close to an exact symmetry.

D. Checks

Allowing the single-particle energies to vary produces more stringent tests of the estimates in Eq. (16). Numerous calculations done for the r_3^n and $(gds)^n$ spaces lead to results that are well summarized by the examples in Table IV.

TABLE IV. Monopole-free $q \cdot q$ calculations in $(gds)^{8-12}$. Single-particle energies in MeV: $\varepsilon_i = [0.0, 0.0, \text{and } 0.0]$ (e0) and $[0.0, 1.0, \text{and } 2.0]$ (e1) for $i = g, d, s$, respectively. "Int" stands for intrinsic values defined in Eq. (16), with $\zeta = 3$.

J	E	Q_s	$BE2$	J	E	Q_s	$BE2$
		$(gds)^8$ e0				$(gds)^8$ e1	
0	−12.977			0	−8.976		
2	0.113	−59.735	857.959	2	0.103	−57.313	795.566
Int	−12.34	−59.98	876.05	Int	−8.28	−57.50	805.07
		$(gds)^{12}$ e0				$(gds)^{12}$ e1	
0	−17.894			0	−12.641		
2	0.125	−65.296	1161.574	2	0.136	−65.609	1065.721
Int	−15.84	−69.16	1165.04	Int	−8.63	−67.49	1109.34

In all cases the self-consistent calculations do well for the quadrupole properties. The estimated energies in $(gds)^8$ are also satisfactory, but they fall short for $(gds)^{12}$, which is triaxial because the platform at $\langle 2q^{20} \rangle = 1.5$ in Fig. 3 is not fully filled, leading to $\mu \neq 0$, while E in Eq. (16) it is designed for $\mu = 0$ only.

V. $N = Z$ NUCLEI

Granted the benefit of some hindsight, a reading of Fig. 3 suggests three regimes for $N = Z$ nuclei from ^{56}Ni up to ^{96}Cd. Note that placing the gds "quasi" orbits on top of the "pseudo" r_3 ones was designed to facilitate such a reading.

(i) *The r_3 pseudo-SU3 nuclei.* They fill orderly the three lowest levels in Fig. 3: ^{60}Zn (analog of ^{20}Ne in the sd shell, a mild rotor), ^{64}Ge (analog of ^{24}Mg, a rotor exhibiting a γ band, as expected whenever orbits are not all filled at a given level), ^{68}Se (analog of ^{28}Si, with degenerate prolate and oblate bands). While SU3 dominance is largely frustrated in the sd shell, here it is expected to hold well because of the near degeneracy of the single-particle orbits. This region makes it possible to study the full pf to r_3 reduction, a unique opportunity to validate the notion of model space and, in particular, the assumption that ^{56}Ni can be treated as a closed shell. As for $r_3 g$ calculations [22], they add little to the r_3 ones.

(ii) *Coexistence from ^{72}Kr to ^{84}Mo.* For 12 particles, i.e., ^{68}Se, $\langle 2q^{20} \rangle$ reaches a maximum in r_3 (see the last lines of Tables I and II). Adding particles to the pseudo orbits leads to a loss while adding them to the quasi orbits leads to a gain. By filling the quasi orbits, well-deformed prolate states can be constructed for 4, 8, 12, and 16 particles whose quadrupole energy will overcompensate the monopole (i.e., single-particle) losses. Oblate states very close in energy can also be found, leading to coexisting bands. The prolate and oblate states demand $r_3 gds$ and $r_3 g$ spaces, respectively. The associated dimensionalities exceed 10^{14} for the former and 10^{10} for the latter, still large but feasible. Therefore, we rely on a generalization of the simplified approach of Sec. IV C for both deformations and check the oblate results via exact diagonalizations. For studies of the region, see Refs. [23,24].

(iii) *The $r_3 g$ nuclei ^{88}Ru, ^{92}Pd, and ^{96}Cd.* The second has been measured recently [25] and postulated as candidate for a new form of boson aligned collectivity. We examine the claim. The—still unknown—spectrum of ^{96}Cd is shown to be probably closer to sdg than to $r_3 g$.

A. The pf-to-r_3 reduction

Doubts may be raised about the doubly magic nature of ^{56}Ni because its first 2^+ is rather low and, depending on the effective interaction used (KB3G, GXPF1A) [26,27], the closed-shell component amounts to only 60%–70%. However, it is in the nature of the shell model to recognize that there may

be a difference between the potentially complicated structure of a state and its simple behavior. As a first hint of what is expected of magic nuclei, we refer to Figs. 1–5 in Ref. [28]: At magic numbers, two-neutron and two-proton separation energies exhibit *systematic* jumps, clearly the case for N or $Z = 28$ and *a fortiori* for ^{56}Ni, but not for occasional candidates such as $N = 56$, which is magic only for $Z = 40$.

For our present purpose the state of interest is the head of the 4p-4h rotational band. According to Eq. (6), four holes in the $0f_{7/2}$ orbit give a prolate contribution of $12b^2$ to the intrinsic quadrupole moment while four pseudo-SU3 particles in r_3 contribute with $\approx 22b^2$, adding up to $34b^2$, in agreement with $32b^2$ from a full 4p-4h pf-shell calculation, a first example of the use of our schematic coupling schemes.

1. $0\hbar\omega$ polarization

The most important characteristic of a doubly magic nucleus is that it defines a before and an after. Before ^{56}Ni, nuclei are basically of f type. Beyond, they are at first of r_3 type until the extension to r_3gds spaces becomes imperative. To treat ^{56}Ni as a core, the Hamiltonian and transition operators have to be renormalized. The dominant mechanism involves coupling to the low-lying 2^+ state, leading to three-body forces and two-body effective transition operators [29] (i.e., state-dependent effective charges), whose neglect, as stressed in Ref. [14], is "common but bad practice." Short of a rigorous treatment, we chose the following expediencies.

(i) For the energies we assume that JUN45 [17] provides a reasonable approximation to the effective Hamiltonian. To fix ideas: In Ref. [14] it is shown that for the quadrupole component of the bare realistic forces the $2\hbar\omega$ effects demand a 30% boost (consistent with what is known about phenomenological interactions). As a consequence, the effective $q \cdot q$ amounts to about 50% of the total interaction. In the case of JUN45 it jumps to over 75%, indicating a strong contribution owing to $0\hbar\omega$ mechanisms.

(ii) For the transition operators we proceed by brute force, estimating effective charges by comparing full pf transitions rates to those obtained in the r_3 or r_3g spaces.

2. ^{60}Zn, more on magicity

To check that ^{60}Zn is properly described by r_3^4 configurations we do a full pf diagonalizations which involves 2 292 604 744 $M = 0$ Slater determinants. The story is told in Table V. A calculation in the r_3 space, using a pure quadrupole-quadrupole interaction, gives values in the range $24b^2$.

As expected, we have good rotational features including $J(J + 1)$ spacings. The full pf-shell calculation using the KB3GR interaction [30] accounts well for the experimental spectrum. The $J(J + 1)$ spacings are gone, but this is of little consequence. As abundantly emphasized in Ref. [3], what matters is the wave function, i.e., the quadrupole moments. The spectrum may be sensitive to details detected in first-order perturbation theory that do not change the structure of the state. The message from Table V is that the quadrupole moments of the huge calculation and the modest one are compatible, to within a crucial caveat: The full pf space leads to Q_{0t} values that are about 1.36 times bigger than the r_3 ones. Because the coupling is mediated basically by the $p_{3/2}f_{7/2}^{-1}$ jumps, the renormalization decreases as the $p_{3/2}$ orbit gets filled, thus blocking the jumps. The results hardly change when JUN45 is used instead of $q \cdot q$ in the $Q_{0t,qq}$ column of Table V: 23 goes to 20.8, increasing the enhancement factor F from 1.36 to 1.48. The calculated spectrum—though still dilated—comes closer to the experimental one.

Note that the evolutions of Q_{0s} and Q_{0t} are quite different. In general, the two quantities will be approximately equal only in the case of well-developed rotors. More often than not, Q_s is very sensitive to details, while Q_t is close to the predictions from Tables I and II.

It is worth mentioning that ^{60}Zn has a superdeformed excited band at relatively low energy with $Q_0 = 67(6)b^2$ [31]. From Tables II and III two prolate candidates emerge with configurations $f^{12}r_3^4(gds)^4$ and $f^{12}(gds)^8$. Both are consistent with observation.

3. ^{64}Ge

For ^{64}Ge the diagonalization of the $q \cdot q$ interaction in the $(r_3)^8$ space yields the expected results for an (84) SU3 representation with nearly degenerate 2^+ states—with Q_0 of equal magnitude and opposite signs—corresponding to the $K = 0$ and 2 ground-state and γ bands, respectively, and $B(E2 : 2^+ \to 0^+)$ of about 300 e^2 fm^4. Table VI proposes a comparison of $q \cdot q$ and JUN45 results—in r_3 and r_3g spaces, respectively—with data, well reproduced by GXPF1A calculations [32]. Using as reference the $B(E2 : 2^+ \to 0^+)$ values, it is found that in going from r_3 to pf the enhancement factors F are 1.62 (for JUN45) and 1.23 (for $q \cdot q$).

TABLE V. Properties of the yrast band of ^{60}Zn (E in MeV, Q in units of b^2). Calculations: full pf with KB3GR; and r_3 with $q \cdot q$.

J	E_{exp}	E_{qq}	E_{pf}	$Q_{0s,qq}$	$Q_{0s,pf}$	$Q_{0t,qq}$	$Q_{0t,pf}$
2^+	1.00	1.00	1.07	24	22	23	31
4^+	2.19	3.34	2.31	23	25	22	30
6^+	3.81	7.03	4.06	23	14	19	31

TABLE VI. Properties of low-lying states in ^{64}Ge: energies in MeV, $B(E2)$ in e^2 fm^4. Calculations: full pf with GXPF1A [32]; r_3g with JUN45; and r_3 with $q \cdot q$.

J^π		Exp	pf	r_3g	$q \cdot q$
2_1^+	E_x	0.90	0.94	0.86	0.50
2_1^+	Q_s		−18.6	−24.4	5.03
	$B(E2 : 2_1^+ \to 0_1^+)$	410(60)	406	251	300
2_2^+	E_x	1.579	1.56	1.27	0.55
2_2^+	Q_s		18.5	23.3	−5.42
	$B(E2 : 2_2^+ \to 2_1^+)$	620(210)	610	182	479
	$B(E2 : 2_2^+ \to 0_1^+)$	1.5(5)	14	13	39
4_1^+	E_x	2.053	2.00	2.16	1.61
	$B(E2 : 4_1^+ \to 2_1^+)$		674	314	390

TABLE VII. Properties of low-lying states in ^{68}Se: energies in MeV, $B(E2)$ in e^2 fm^4. Calculations: full pf with GXPF1A [32]; r_3 with JUN45: r_3 with $q \cdot q$; and full pf with KB3GR (PF). The experimental 0_2^+ energy is a guess.

J^π		Exp	pf	r_3	$q \cdot q$	PF
0_2^+	E_x	(1.19)	0.69	0.96	0.79	1.42
2_1^+	E_x	0.85	0.71	0.54	0.53	0.96
2_1^+	Q_s		11	35	−42	39
	$B(E2 : 2_1^+ \to 0_1^+)$	440(60)	491	307	420	409
2_2^+	E_x	1.59	1.00	1.39	1.26	1.74
2_2^+	Q_s		−8	−33	42	−16
	$B(E2 : 2_2^+ \to 2_1^+)$		689	7	0.00	297
	$B(E2 : 2_2^+ \to 0_2^+)$		499	262	420	223
	$B(E2 : 2_2^+ \to 0_1^+)$	0.3	4	0.7	0.00	10
4_1^+	E_x	1.94	1.66	1.61	1.77	1.86
4_1^+	Q_s		59	43	−53	63
	$B(E2 : 4_1^+ \to 2_1^+)$		590	419	565	810
4_2^+	E_x	2.55	1.98	2.28	2.37	2.79
4_2^+	Q_s		−51	−42	53	−14
	$B(E2 : 4_2^+ \to 2_2^+)$		510	354	565	154

4. ^{68}Se: The double platform

The structure of $N = Z$ even nuclei from $A = 72$ to 84 is described by piling up $(gds)^4$ blocks on top r_3^{12}, i.e., on top of either the oblate and prolate ground-state bands—corresponding to the (12, 0) and (0, 12) SU3 representations—of ^{68}Se, which becomes a common "double platform" (refer to Fig. 3). Hence the importance of this nucleus to fix the e_0 effective charge.

From Table I the estimate $Q_0/b^2 = \pm 33.2$, i.e., $B(E2 : 2^+ \to 0^+) \approx 414$ e^2 fm^4 , consistent the $q \cdot q$ numbers in Table VII, which also collects JUN45 results in r_3, the full pf GXPF1A and KB3GR ones (labeled pf and PF, respectively) and data including the only experimentally known $B(E2 : 2^+ \to 0^+) = 440(60)$ e^2 fm^4.

With the exception of the $B(E2 : 2_2^+ \to 2_1^+)$ the calculations in r_3 and pf are quite consistent, with enhancement factors $F \approx 1.16$ and 1.38 for the $q \cdot q$ and JUN45 numbers, respectively. The KB3GR interaction yields somewhat better spectra than GXPF1A, and similar quadrupole properties except for the $J = 2_2^+$ and 4_2^+ states that are more mixed for the latter.

Using the $2\hbar\omega$ value $e_0 = 1.77$ [14], the $0\hbar\omega$ contribution increases it to $e_0 = 1.77\sqrt{F} \approx 2.1 \pm 0.1$. When gds particles come into play their quadrupole operators will also couple with the $J = 2^+$ state in ^{56}Ni, though more weakly owing to larger norm denominators [see Eqs. (9) and (17)]. It is hoped that the associated suppression can be accommodated by the proposed estimate.

The JUN45 calculation in $r3g$ leads to a ground state that is 60% 0p-0h, 30% 2p-2h, and 10% 4p-4h. As can be gathered from Tables I and II, these admixtures bring no extra oblate coherence, but with the same numbers prolate contributions could make a difference in a full r_3gds calculation. VAMPIR calculations [33] indicate substantial oblate-prolate mixing in the ground-state band. Further data on this nucleus could be of interest.

TABLE VIII. Properties of $r_3^k(gds)^l$ configurations. Total (E), quadrupole (E_q), and single-particle (hsp) energies from Eq. (18) with $\zeta = 0$, in MeV; quadrupole moment $Q_4 = \langle 2q_{20(4)}\rangle$; $BE2 = B(E2 : 2^+ \to 0^+)$ in e^2 fm^4 from Eq. (17); $\beta = 8$ in Eq. (14). For prolate states Q_4 is the calculated one. For oblate states the space is $r_3^k(g)^l$, so $\epsilon_{r_3} = 0.0$ and Q_4 (not shown) is from Table II. Q_3 is always from Table II. Energies of triaxial states are in boldface. Single-particle energies in MeV: $\varepsilon_i = 0.0$, 3.0, and 4.0 [0.0, 4.0, and 5.0] for $i = g, d, s$, respectively, and $\epsilon_{gr} = 2.5$ [2.0]. Numbers in square brackets apply to the last two lines only.

k	l	A	E	$-E_q$	hsp	Q_3	Q_4	$BE2$
12	4	72	−12.29	25.53	3.24	30.20	23.00	1225
16	0	72	−8.37	8.37	0.0			324
12	4	72	−10.63	20.63	0.0			939
12	8	76	−12.29	40.05	7.76	30.20	41.17	2212
16	4	76	−2.46	15.62	3.15	20.72	22.85	867
14	6	76	−4.90	19.90	0.0			987
16	4	76	−6.23	16.23	0.0			805
12	12	80	**−0.30**	47.01	16.71	30.20	49.15	2792
16	8	80	1.76	27.45	7.69	20.72	41.17	1733
18	6	80	−0.04	15.04	0.0			823
12	16	84	5.91	51.92	17.82	30.20	54.71	3271
16	12	84	**13.47**	33.20	16.67	20.72	49.01	2240
20	8	84	6.05	13.95	0.0			840
12	16	84	3.02	51.25	22.26	30.20	54.05	3223
20	8	84	2.05	13.95	0.0			840

B. The central region: $A = 72$ to 84

Let us recast E in Eq. (17) so as to separate the two basic contributions to the monopole term H_m,

$$E = \sum \varepsilon_{i=g,d,s} \langle n_i \rangle + l(\varepsilon_g - \varepsilon_{r_3})$$
$$- \hbar\omega\kappa \left(\frac{Q_3}{15} + \frac{Q_4}{23} \right) \left(\frac{Q_3 + \zeta}{15} + \frac{Q_4 + \zeta}{23} \right)$$
$$= hsp + l\epsilon_{gr} + E_q, \quad (18)$$

where we have introduced the notations used in Table VIII—the core of this study— which lists the properties of the dominant and subdominant prolate and oblate states.

To ascertain the stability of the estimates, all the calculations, done with $\zeta = 0$, have been redone for $\zeta = 3$. The examples that follow are for $A = 84$, which involves the largest magnitudes for hsp, $l\epsilon_{gr}$, and E_q and hence, presumably, the largest uncertainties.

For $\zeta = 0 \to 3$ the energies $E = 5.91$, 13.47, and 6.05 in Table VIII go to 4.03, 11.89, and 5.0, respectively, leaving unchanged the qualitative conclusions that may be drawn.

The evolution of the monopole is another source of uncertainty: The ε_i and ε_{gr} numbers are suggested by GEMO [34] at the beginning of the region. As the g filling increases, the orbit will separate from its ds partners and come closer to the r_3 space. To simulate this effect, in the last two lines of Table VIII the single-particle energies are changed to the bracketed values in the caption. As a consequence the energies at $E = 5.91$ and 6.05 change to 3.02 and 2.05, respectively. Again the qualitative conclusions are not affected.

These results for ^{84}Mo are typical and illustrate two important points.

(1) For prolate states $B(E2 : 2^+ \to 0^+)$ and $\langle 2q^{20} \rangle$ are very unsensitive to monopole behavior and hence remain close to their theoretical quasi + pseudo-SU3 maxima. In our example $Q_4 = 54.71$ and 54.05 against the 55.88 maximum.

(2) Energies of prolate states are very sensitive to the single-particle field $H_{\rm sp}$. In our example there is a shift of some 4.5 MeV: $hsp = 17.82$ vs 22.26 MeV. However, the relative positions of the states remain fairly stable.

Examine now what conclusions can be drawn from Table VIII.

^{72}Kr. This is the only species where $B(E2 : 2^+ \to 0^+)$ are close for prolate and oblate candidates. Probable coexistence.

^{76}Sr. There is a single candidate. It is an experimentally superb rotor with good $J(J + 1)$ sequence, in perfect agreement of Table VIII with a recent measure: $B(E2, 2^+ \to 0^+) = 2220(270)$ e^2 fm^4 [35].

^{80}Zr. The lowest state is expected to gain some 4 MeV because of triaxiality and the observed rotational spectrum seems to guarantee $B(E2 : 2^+ \to 0^+)$, close to the prediction. However, the very low-lying oblate state may blur the picture. Moreover, the prolate 8p-8h (and a 10p-10h, not shown) are also close and triaxial. Finally, the frustrated doubly magic $N = Z = 40$ is at 0 MeV. This is a very interesting nucleus.

^{84}Mo. There is a strong hint of coexistence, even triple coexistence through gains owing to triaxiality of the second prolate candidate.

Except for ^{76}Sr, coexistence is expected in the other nuclei and is examined in Sec. VI.

C. The r3g calculations

Calculations in the $(r_3g)^n$ spaces have been carried out for all n. We concentrate on results for $A \geqslant 80$. In particular, ^{80}Zr and ^{84}Mo are mainly of interest in lending support to a basic observation about oblate bands.

Contrary to prolate states that privilege maximizing the deformation, the oblate bands give precedence to mixing that reduces it. As a consequence, our schematic estimates overestimate $\langle 2q^{20} \rangle$ and $B(E2 : 2^+ \to 0^+)$ and underestimate energies.

1. ^{80}Zr and ^{84}Mo

In Table IX the extracted $Q_0 \approx 180$ is definitely lower than the 6p-6h number from Table II, $Q_0 \approx (19 + 23 + 3)b^2 \approx 203$ e fm^2 . The wave functions have 22% 4p-4h, 44% 6p-6h, and

TABLE IX. ^{80}Zr. Results of the full (1.1×10^{10}-dimensional) r_3g calculation with JUN45 (E's in MeV, Q in e fm^2 and $B(E2 : 2^+ \to 0^+)$ in e^2 fm^4).

J	$E(2^+)$	Q_s	Q_{0s}	$B(E2)$	Q_{0t}^2
2	0.393	51	-179	642	$(180)^2$

TABLE X. ^{84}Mo. Properties of the yrast band; experiment vs calculations in the r_3g space with the JUN45 interaction: To the left, truncated up to four holes in r_3; to the right, complete space [E in MeV, Q in e fm^2, and $B(E2)$ in e^2 fm^4]. E_x and E_t stand for experimental and theoretial energies respetively.

J	Ex	Et	$-Q_{0s}$	$B(E2)$	$-Q_{0t}$	Et	$-Q_{0s}$	$B(E2)$	$-Q_{0t}$
0	0.0	0.0				0.00			
2	0.44	0.17	194	762	196	0.29	189	708	188
4	1.12	0.56	190	1081	195	0.84	189	1020	189
6	2.01	1.15	184	1179	194	1.60	189	1118	189

28% 8p-8h. Mixing with prolate states nearby may be at the origin of the reduction, as confirmed in Table X for ^{84}Mo.

The ground-state band is dominated now by the $r_3^{-4}g^8$ configuration. From Table II, $Q_0 \approx (21 + 20 + 3)b^2 = 44 \times 4.61 \approx 203$ e fm^2, not inconsistent with the *truncated* calculations (left part of the table) that exhibit good rotational features. Once the full space is incorporated (right part of the table), the energies depart from the $J(J + 1)$ sequence, while the quadrupole properties, still those of a rotor, have suffered an erosion owing to the inclusion of prolate states as suggested in ^{80}Zr.

2. ^{88}Ru

In ^{88}Ru we come at last to a genuine r_3g nucleus. (Note that for $A \geqslant 88$ most numerical results reported below duplicate those of the Rutgers group [36].) Table XI corresponds to an yrast oblate band exhibiting 50% $r_3^{-4}g^{12}$ oblate dominance. This is not obvious, because g^{12} is now beyond midshell and the largest $\langle 2q^{20} \rangle$ is prolate. However, the oblate $\langle 2q^{20} \rangle$ in r_3^{-4} is sufficiently strong to dominate but the prolate admixtures distort and reduce the original $\langle 2q^{20} \rangle = -(18.66 + 20.24)$ and $Q_0 \approx -182$ to $Q_{0s} \approx -125$ and $Q_{0t} \approx -160$ in Table XI. It is seen that in this nucleus the prolate-oblate competition within the r_3g space is played up. ^{92}Pd will bring further news.

3. ^{92}Pd

The authors' interest in heavy $N = Z$ nuclei was sparked by the first measurement of the ^{92}Pd spectrum, accompanied by an interpretation that associated it with a condensate of $(g_{9/2}^2)$ neutron-proton pairs coupled to maximum $J = 9$ [25,37,38]. This raised two issues: that of possible coupling schemes in a g^{12} space and that of possible dominance of this configuration.

TABLE XI. Properties of the yrast band of ^{88}Ru: experiment vs calculations in the r_3g space with the JUN45 interaction [E in MeV, Q in efm^2, and $B(E2)$ in e^2 fm^4].

J	E(exp)	E(th)	Q_s	$B(E2 \downarrow)$(th)
0_1^+	0.0	0.0		
2_1^+	0.62	0.56	37	492
4_1^+	1.42	1.31	44	766
6_1^+	2.38	2.12	47	888
8_1^+	3.48	2.88	52	980

TABLE XII. Properties of ^{92}Pd. Energies in MeV, Q in e fm^2 and $B(E2)$ in e^2 fm^4. Detailed explanation in text.

1	2	3	4	5	6	7	8	9	10
J	Ex	Et	Con	qq	Ω	$B(E2)$	$B(E2)_{r_3g}$	Q_s	Q_{s,r_3g}
0	0.0	0.0	0.00	0.00	0.99	–	–	–	–
2	0.874	0.84	0.26	0.22	0.99	225	304	−28	−3.63
4	1.786	1.72	0.58	0.62	0.99	316	382	−34	−8.20
6	2.563	2.52	0.85	1.20	0.98	340	364	−31	−2.77

TABLE XIII. ^{96}Cd. Energies in MeV, Q in e fm^2 and $B(E2)$ in e^2 fm^4 e^2 fm^4.

J^π	ΔE			$B(E2)$			Q_s		
	r_3g	$g_{9/2}$	sdg	r_3g	$g_{9/2}$	sdg	r_3g	$g_{9/2}$	sdg
0^+	0.0	0.0	0.0						
2^+	0.90	0.96	0.77	152	154	327	−19	−23	−37
4^+	1.91	2.10	1.78	203	206	426	−22	−22	−40
6^+	3.02	3.08	2.78	191	159	351	−11	−5	−23
8^+	3.48	3.08	3.24	47	40	65	40	39	55

Table XII —which we comment column by column—sums up sufficient information to resolve both issues:

(1) J value;
(2) experimental spectrum, in very good agreement with 3;
(3) JUN45 spectrum;
(4) spectrum of the condensate defined by $-H_{\mathrm{con}} = P_0 + 9P_9$, where P_0 and P_9 are the pairing Hamiltonians for $J = 0$ and 9;
(5) spectrum of the quadrupole force scaled so as to have unit $J = 9$ matrix element, close to that of the condensate (within arbitrary scaling factor);
(6) overlap, $\Omega = \langle qq|\mathrm{con}\rangle^2$, of the wave functions indicating that the condensate and quadrupole coupling schemes are identical (the use of P_9 should be understood as an artifact to define a coupling scheme; as a Hamiltonian it is better avoided);
(7, 8) a Hamiltonian $-H \approx 0.6qq + 0.4P_0$ yields g^{12} energies that are close to the exact ones and $B(E2)$ that are very close to the pure qq values in column 7 and not too far from the exact ones in column 8, which may encourage the idea of g^{12} dominance in spite of its smallish 30% contribution to the exact wave function (however, this idea is not supported by the disparity of Q_s in columns 9 and 10);
(9, 10) spectroscopic Q_s for qq (9) and JUN45 [17] (10).

The situation is reminiscent of that of $f_{7/2}^n$ configurations that yield apparently reasonable energetics and transition rates but quadrupole moments of the wrong sign [39].

The pattern we started following at ^{80}Zr—of oblate states progressively eroded by prolate mixtures—now reaches its climax with the Pyrrhic victory of prolate states practically canceled by oblate mixtures.

4. ^{96}Cd

For this nucleus, the calculations in the r_3g and g spaces with JUN45 give results that are much closer than in ^{92}Pd, both for the energies and for the $B(E2)$ properties and the discrepancies in the spectroscopic quadrupole moments are gone except for the 6^+ state.

We have collected some results in Table XIII, adding those from the full sdg space using the Nowacki-Sieja interaction [40], which describes the superallowed decay of ^{100}Sn [41] and the $B(E2)$ systematics of the light Sn isotopes [42]. The results for the energies, $B(E2)$ and Q values vary little between g and r_3g, pointing to g dominance, not

invalidated by the substantial quadrupole coherence brought in by the full sdg space calculation as it amounts basically to an overall scaling.

It is worth mentioning that the latter predicts a 16^+ isomer at 5.3 MeV.

VI. CASE STUDIES, COMPARISONS, AND PERSPECTIVES

The central region calls for some extra comments.

A. Coexistence in ^{72}Kr

Exact $(r_3g)^{16}$ calculations with JUN45 [17] for ^{72}Kr indicate that—with respect to Table VIII—the gap $r_3^{12}g^4 - r_3^{16}$ is underestimated by about 2 MeV, while $B(E2 : 2^+ \to 0^+)$ is overestimated by 10%. The ground-state band is a nice oblate rotor with nearly constant $Q_{ot} \approx 205\, e$ fm^2, good $J(J+1)$ sequence with the 2^+ at 350 keV—half the observed value— while the 4^+ at 1.1 MeV is close to the observed 1.32 MeV, while $B(E2 : 2^+ \to 0^+) = 850\ e^2$ fm^4 against a measured 999(129) e^2 fm^4 [43]. In this reference it is argued that the ground band is oblate. A suggestion that may gain some support from the shape of the Gamow-Teller β^+ decay strength function [44]. Recent measures [45] yield $B(E2 : 2_1 \to 0_1) = 810(150)\ e^2$ fm^4 (too small to be prolate) and $B(E2 : 4_1 \to 2_1) = 2720(550)\ e^2$ fm^4 (too large to be oblate, even large for prolate in view of theoretical maximum of 2200 e^2 fm^4. (Note that an analysis of Fig. 3 of [45] suggests that the 550 e^2 fm^4 error bar is underestimated.)

Clearly, some mixing is necessary and to achieve it we resort to the space which is the largest we could treat and the smallest that could cope with prolate states, i.e., $r_3^{16-t}(gd)^t$, tractable for $t \leqslant 4$. The interaction chosen is R3GD, i.e., JUN45 supplemented by matrix elements involving the d orbit from the LNPS set [46].

First, two calculations at fixed $t = 4$ were made. If the single-particle energy ε_d is set 1.76 MeV above ε_g, the ground-state band is solidly prolate. If the splitting is increased by 0.5 MeV the lowest $J = 0^+$ and 2^+ become oblate, but the lowest 4^+ is prolate and nearly degenerate with its oblate counterpart. The two bands simply slide past, ignoring each other. To achieve any mixing, extreme fine tuning is required.

Things change when configuration mixing is allowed. In Table XIV, to the left, is the result at fixed $t = 4$ with prolate ground state ($\varepsilon_d - \varepsilon_g = 1.76$ MeV). The choice is made to present the two bands in their pure form. To the right, the

TABLE XIV. Properties of the yrast bands of ^{72}Kr calculated in the r_3gd space with the R3GD interaction (see text) [E's in MeV, Q in $e\,fm^2$, and $B(E2) \equiv B(E2 : J_i \to J_{fx})$ in $e^2\,fm^4$]. Bottom: first line, measured values from [45] (error bars subject to caution as explained in text); second line, $t \leqslant 4$ results boosted as explained in the text.

| | $t = 4$ | | | | $t \leqslant 4$ | | | |
| | | | | $B(E2)$ | | | | $B(E2)$ |
J_i	Ex	Q_s	J_{f1}	J_{f2}	Ex	Q_s	J_{f1}	J_{f2}
0_1	0.0				0.00			
0_2	0.24				0.30			
2_1	0.28	-65	1089	6	0.46	-54	586	372
2_2	0.56	58	3	897	0.66	45	103	536
4_1	0.83	-77	1509	1	1.05	-75	1387	75
4_2	1.23	69	0	1286	1.43	64	36	1093

$B(E2 : 2_1 \to 0_1) = 810(150)$, $\quad B(E2 : 4_1 \to 2_1) = 2720(550)$
$t \leqslant 4 \times 1.4$; $\quad B(E2 : 2_1 \to 0_1) = 740$, $B(E2 : 4_1 \to 2_1) = 1750$

$t \leqslant 4$ results show prolate dominance with strong ground-state mixing, using $\varepsilon_d - \varepsilon_g = 2.26$ MeV, which yields oblate ground state at fixed $t = 4$. While $B(E2 : 2^+ \to 0^+)$ is halved, the $B(E2 : 4_1^+ \to 2_1^+)$ changes by less than 10%. To estimate the effect of omitting the s orbit, we redo calculations as in Table VIII: $\varepsilon_d = 2$ MeV and no s orbit, and then add $\varepsilon_s = 3$ MeV. The rates are boosted 15%, and a further 10% may come from $e_0 = 2.1$, as suggested near the end of Sec. V A 4, for a total of 26%. At the bottom of Table XIV the corresponding boosted values are compared with the observed ones.

Let us add two entries to the list of calculations quoted by Iwasaki and co-workers [45], which fall in two groups.

(i) *Those that mix prolate and oblate states.* They include VAMPIR [47]—which produces thorough mixing as a reassessment of oblate dominance previously predicted [23]—and the relativistic mean-field work of Fu *et al.* [48], close to the present results: strong $0_1^+ \pm 0_2^+$ mixing and strong prolate dominance in 2_1^+.
(ii) *Those that predict oblate ground bands.* They include Skyrme [24,49] and Gogny [50,51] (beyond) mean-field approaches and a sophisticated form [52] of the Kumar-Baranger model in two major oscillator shells [21].

In Sec. VI B it is explained why a majority of calculations privilege the oblate solution.

Digression. Gamow-Teller strength calculated with the present wave functions agrees nicely with observation.

B. Monopole vs single-particle field

Most mean-field-based calculations have single-particle spectra in which the d orbit is some 5 MeV above the g one (as in Fig. 1 of Ref. [53]), i.e., some 2 MeV above the values in Table VIII. As emphasized in Ref. [11] and Sec. II, H_m is a strict two-body operator, but its action can be simulated by single-particle fields—provided it is understood that they vary as a function of the orbital occupancies—the "monopole drift" mostly owing to the filling of the largest j orbit in a major shell [54]. In the problems studied here, the r_3 space can be

viewed as frozen, but the gds orbits are subject to drift. Above ^{56}Ni the r_3 orbits are nearly degenerate and the gds ones are close to an $l \cdot s$ sequence. There is no direct experimental evidence for the position of the ds orbits around $A = 68$, but we can rely on the GEMO program [34], which accounts for the particle or hole spectra on all known double magics to within 200 keV and confirms the $l \cdot s$ behavior with the d orbit 2–3 MeV above the g one, which upon filling comes closer to r_3 and becomes detached from ds, which move up to join their r_4 partners to form a pseudo-LS scheme.

In ^{72}Kr, as elsewhere, the structure of the states is unsensitive to monopole details but their energies are not, which explains why so many calculations place the prolate state too high.

C. Potential energy surfaces in ^{80}Zr

In the comments to Table VIII it was noted that to the three states included for ^{80}Zr one should add a 10p-10h, $r_3^{14}(gds)^{10}$ prolate state at about 1 MeV with $B(E2 : 2^+ \to 0^+) \approx 2100$ $e^2\,fm^4$ and the r_3^{24} closed shell at 0 MeV. Because the three prolate states are triaxial they will gain energy (of the order of 3–4 MeV according to Table IV) and dominate the low-lying spectrum. In the thorough study of Rodríguez and Egido with a Gogny force (Ref. [53], Fig. 3) this is very much the case. The main discrepancy with their work is in the positioning of the closed shell, which in the potential energy surface (Ref. [53], Fig. 2) comes some 4 MeV below the deformed minima, which we attribute to underbinding of the latter owing to the monopole effect described above. Other calculations for ^{80}Zr include Refs. [23,24,55].

D. Coexistence in ^{84}Mo

According to Refs. [23,24] the ground state of ^{84}Mo is prolate and spherical, respectively. Table VIII suggests three candidates:

(I) a splendid axial rotor (all "platforms" filled in the ZRP diagrams in Fig. 3), expected to have a 2^+ well below the observed 440 keV;
(II) a splendid oblate rotor (Table X) whose 2^+ is way too low;
(III) a triaxial rotor.

No direct information is available, but ^{82}Zr, whose behavior is likely to be similar, provides a hint. Collating data from Refs. [56–58], the ground state starts with 2^+ at 407 keV and $B(E2 : 2^+ \to 0^+) \approx 1900$ $e^2\,fm^4$, is interrupted by a definitely smaller $B(E2 : 4^+ \to 2^+)$ at 700–1200 $e^2\,fm^4$, and then resumes with a fairly constant Q_0, albeit smaller than the one extracted from $B(E2 : 2^+ \to 0^+)$. Our guess is prolate dominance in ^{84}Mo quenched by mixing.

E. Beyond intrinsic states

In mean-field studies, "going beyond" amounts to projecting and moving in the β-γ plane. Here we do not have a potential energy surface but a space of discrete intrinsic states: The numerous local minima, revealed by Tables I and II, constitute a natural basis in which pairing will act as mixing

agent. We do not know yet how to do the mixing, but we may call attention to a way of dealing with each individual state.

Diagonalize separately in the quasi and pseudo spaces and then recouple in the product space. There is nothing new with this "weak-coupling" idea except one thing: The quadrupole force(s) used in each space must be boosted as much as necessary to reproduce the quadrupole moments dictated by the MZ calculations.

VII. LOOKING BACK AND FORWARD

The paper contains at least three significant results: (A) the numerical suggestion that pseudo-SU3 may behave as an exact symmetry (Table III) using the true quadrupole force rather than its pseudo counterpart; (B) the pf to r_3 reduction in Sec. V A (we have seized a unique opportunity to study the projection from a very large realistic space into a sensible model one); (C) most important, the operation of the quasi-pseudo-SU3 tandem, which was shown to account for the onset of rotational motion in the rare earths, involving the $r_4 hfp$ (proton) and $r_5 igds$ (neutron) EEI spaces [3].

The formal basis of this successful estimate was not clear at the time. Now it can be ascribed to Nilsson-SU3 self-consistency that puts together the two classics in the field: the Bohr-Mottelson rotational model [13] plus Elliott's quadrupole force and SU3 symmetry [1], via a reinterpretation of the Nilsson model [2]. Equation (19) makes explicit the connections

$$H = H_{\rm sp} - \frac{\hbar\omega\delta}{3} 2q_0 \equiv H_{\rm sp} - \beta\hbar\omega\kappa \frac{\langle 2q_0 \rangle}{\mathcal{N}^2} 2q_0. \quad (19)$$

On the left-hand side, the Nilsson problem amounts to calculating single-particle energies in the presence of a deformation δ. The constraints on δ were left undefined and the earliest successful calculation of quadrupole moments relied on volume conservation [59]. It was much later that the Nilsson orbits could be associated with an energy minimization [21,60].

On the right-hand side of Eq. (19) we have summed up the self-consistent formulation—the MZ Eqs. (13) and (14)—with its built-in constraint: The input $\langle 2q^{20} \rangle$ must coincide with the output $\langle 2q^{20} \rangle$. The emphasis is on the quadrupole moment, not the energy: Nilsson orbits are sensitive to the central field, while "$\langle 2q^{20} \rangle$ orbits," i.e., the ZRP diagrams in Fig. 3, are nearly constant, reflecting the underlying operation of pseudo-quasi-SU3. The resulting interpretive framework explains the appearance of "closed shells" [the $(\lambda 0)$ representations], the natural prolate dominance, the importance of "triaxiality" [the $(\lambda\mu)$ representations], and the abrupt departure from the pf regime beyond $A = 68$.

The open task is to put the energetics on firmer ground, while trying to keep the approach simple, or, at least, computationally doable.

Notes on authorship. A.P.Z. designed, wrote, and contributed to all sections. All authors contributed to Secs. V A and V C. A.P. contributed to the original formulation of the paper and to Secs. III and VI A. S.M.L. contributed to Sec. II.

[1] J. P. Elliott, Proc. R. Soc. London, Ser. A **245**, 128 (1956).

[2] S. G. Nilsson, Mat. Fys. Medd. Dan. Vid. Selsk **29**, 16 (1955).

[3] A. P. Zuker, J. Retamosa, A. Poves, and E. Caurier, Phys. Rev. C **52**, R1741 (1995).

[4] Unless explicitly noted, all experimental information comes from http://www.nndc.bnl.gov/ensdf and http://www.nndc.bnl.gov/be2

[5] A. P. Zuker, B. Buck, and J. B. McGrory, Phys. Rev. Lett. **21**, 39 (1968); A. P. Zuker, *ibid.* **23**, 989 (1969).

[6] P. Navratil and W. E. Ormand, Phys. Rev. Lett. **88**, 152502 (2002).

[7] A. P. Zuker, Phys. Rev. Lett. **90**, 042502 (2003).

[8] J. Mendoza-Temis, J. Hirsch, and A. P. Zuker, Nucl. Phys. A **843**, 14 (2010).

[9] T. Otsuka, T. Suzuki, J. D. Holt, A. Schwenk, and Y. Akaishi, Phys. Rev. Lett. **105**, 032501 (2010)

[10] A. Schwenk and A. P. Zuker, Phys. Rev. C **74**, 061302 (2006).

[11] E. Caurier, G. Martínez-Pinedo, F. Nowacki, A. Poves, and A. P. Zuker, Rev. Mod. Phys. **77**, 427 (2005).

[12] C. J. Lister *et al.*, Phys. Rev. Lett. **59**, 1270 (1987).

[13] A. Bohr and B. Mottelson, Mat. Fys. Medd. Dan. Vid. Selsk **27**, 16 (1953).

[14] M. Dufour and A. P. Zuker, Phys. Rev. C **54**, 1641 (1996).

[15] A. Arima, M. Harvey, and K. Shimizu, Phys. Lett. B **30**, 517 (1969); K. Hecht and A. Adler, Nucl. Phys. A **137**, 129 (1969).

[16] G. Martínez-Pinedo, A. P. Zuker, A. Poves, and E. Caurier, Phys. Rev. C **55**, 187 (1997).

[17] M. Honma, T. Otsuka, T. Mizusaki, and M. Hjorth-Jensen, Phys. Rev. C **80**, 064323 (2009).

[18] G. Martínez-Pinedo and A. P. Zuker, Nilsson and self-consistent Nilsson programs (unpublished).

[19] J. Retamosa, J. M. Udias, A. Poves, and E. Moya de Guerra, Nucl. Phys. A **511**, 221 (1990).

[20] H. L. Crawford *et al.*, Phys. Rev. Lett. **110**, 242701 (2013).

[21] M. Baranger and K. Kumar, Nucl. Phys. A **110**, 490 (1968).

[22] K. Kaneko, M. Hasegawa, and T. Mizusaki, Phys. Rev. C **70**, 051301(R) (2004).

[23] A. Petrovici, K. W. Schmid, and A. Faessler, Nucl. Phys. A **605**, 290 (1996).

[24] M. Yamagami, K. Matsuyanagi, and M. Matsuo, Nucl. Phys. A **693**, 579 (2001).

[25] B. Cederwall *et al.*, Nature (London) **469**, 69 (2011).

[26] A. Poves, J. Sánchez Solano, E. Caurier, and F. Nowacki, Nucl. Phys. A **694**, 157 (2001).

[27] M. Honma, T. Otsuka, B. A. Brown, and T. Mizusaki, Eur. Phys. J. A **25**, 499 (2005).

[28] G. Dussel, E. Caurier, and A. P. Zuker, At. Data Nucl. Data Tables **39**, 205 (1988).

[29] A. Gottardo *et al.*, Phys. Rev. Lett. **109**, 162502 (2012).

[30] E. Caurier and A. Poves (unpublished).

[31] C. E. Svensson *et al.*, Phys. Rev. Lett. **82**, 3400 (1999).

[32] K. Starosta *et al.*, Phys. Rev. Lett. **99**, 042503 (2007).

[33] A. Petrovici, K. W. Schmid, and A. Faessler, Nucl. Phys. A **710**, 246 (2002).

[34] J. Duflo and A. P. Zuker, Phys. Rev. C **59**, R2347 (1999); and program GEMO in amdc.in2p3.fr/web/dz.html

[35] A. Lemasson *et al.*, Phys. Rev. C **85**, 041303(R) (2012).

[36] S. J. Q. Robinson, T. Hoang, L. Zamick, A. Escuderos, and Y. Y. Sharon, Phys. Rev. C **89**, 014316 (2014).

[37] C. Qi, J. Blomqvist, T. Back, B. Cederwall, A. Johnson, R. J. Liotta, and R. Wyss, Phys. Rev. C **84**, 021301 (2011).

[38] S. Zerguine and P. Van Isacker, Phys. Rev. C **83**, 064314 (2011).

[39] A. Poves and A. Zuker, Phys. Rep. **70**, 235 (1981).

[40] N. Singh *et al.*, Phys. Rev. Lett. **107**, 172502 (2011).

[41] C. B. Hinke *et al.*, Nature (London) **486**, 341 (2012).

[42] G. Guastalla *et al.*, Phys. Rev. Lett. **110**, 172501 (2013).

[43] A. Gade *et al.*, Phys. Rev. Lett. **95**, 022502 (2005).

[44] P. Sarriguren, Phys. Rev. C **79**, 044315 (2009).

[45] H. Iwasaki *et al.*, Phys. Rev. Lett. **112**, 142502 (2014).

[46] S. M. Lenzi, F. Nowacki, A. Poves, and K. Sieja, Phys. Rev. C **82**, 054301 (2010).

[47] A. Petrovici, K. W. Schmid, and A. Faessler, Nucl. Phys. A **665**, 333 (2000).

[48] Y. Fu, H. Mei, J. Xiang, Z. P. Li, J. M. Yao, and J. Meng, Phys. Rev. C **87**, 054305 (2013).

[49] M. Bender, P. Bonche, and P.-H. Heenen, Phys. Rev. C **74**, 024312 (2006).

[50] M. Girod, J.-P. Delaroche, A. Görgen, and A. Obertelli, Phys. Lett. B **676**, 39 (2009).

[51] T. R. Rodríguez, Phys. Rev. C **90**, 034306 (2014).

[52] K. Sato and N. Hinohara, Nucl. Phys. A **849**, 53 (2011).

[53] T. R. Rodríguez and J. L. Egido, Phys. Lett. **705**, 255 (2011).

[54] A. P. Zuker, Nucl. Phys. A **576**, 65 (1994).

[55] S. J. Zheng, F. R. Xu, S. F. Shen, H. L. Liu, R. Wyss, and Y. P. Yan, Phys. Rev. C **90**, 064309 (2014).

[56] A. A. Chishti *et al.*, Phys. Rev. C **48**, 2607 (1993).

[57] S. D. Paul, H. C. Jain, and J. A. Sheikh, Phys. Rev. C **55**, 1563 (1997).

[58] D. Rudolph *et al.*, Phys. Rev. C **56**, 98 (1997).

[59] B. Mottelson and S. G. Nilsson, Mat. Fys. Skr. Dan. Vid. Selsk 1 (1959): No-8.

[60] V. M. Strutinsky, Nucl. Phys. A **122**, 1 (1968).